The van Hemmen Spin Glass Model on Scale-Free Networks

Do-Hyun Kim[1,*] and B. Kahng[2,†]

[1] *Department of Physics, Sogang University, Seoul 04107, Korea*
[2] *Department of Physics and Astronomy, Seoul National University, Seoul 08826, Korea*

We study the so-called van Hemmen spin glass (vHSG) model on scale-free (SF) networks without replicas. The vHSG model contains two types of coupling terms: a ferromagnetic coupling term with strength J_0 and a quenched random exchange coupling term with strength J. The ratio J_0/J is the relative strength between the ferromagnetic (F) and the spin glass (SG) interactions. The degree exponent λ and mean degree K of SF networks, as well as the temperature T, are control parameters. We construct phase diagrams based on the analytic solutions of phase boundaries among the F, SG, mixed (M), and paramagnetic (P) phases. When $\lambda = \infty$, the obtained phase diagram is the same as that of the original vHSG model, consisting of all those phases. When λ is decreased but greater than three, the phase boundaries are deformed but all the phases exist. However, when $2 < \lambda < 3$, the P phase disappears but the SG phase exists only at $J_0 = 0$. The M and F phases prevail. One of the distinct features of the vHSG model is the occurrence of a first-order transition curve and critical endpoint (CE) at which a second-order transition curve terminates in the first-order transition curve. At the CE, a hybrid phase transition occurs in which properties of the second-order and first-order transitions emerge simultaneously. This feature does not occur in the SG model with replicas. The exponent of the SG order parameter is different from that obtained from the replica method. We anticipate that the phase diagram and the features of the phase transitions we obtained here would be helpful to understand emerging patterns from socio-complex systems.

PACS numbers: 89.75.Hc, 89.65.s, 89.75.Fb, 75.10.Nr

I. INTRODUCTION

A spin glass (SG) model has served as a paradigmatic model to understand the physical properties of composite materials with frustrating interactions for a long time [1]. Recently, however, the SG model has resurged in the area of complex networks, because it can be used for understanding emerging patterns from social conflicts between people. Social relations among people are represented using networks, in which nodes and links in the networks represent individuals and their interactions, respectively. Social networks are often scale-free (SF) networks of which the distribution of degrees follows a power law, $P_d(k) \sim k^{-\lambda}$. Here, the degree of a certain node i is the number of its neighbors, k_i. One may naively think that the solution of the SG model for SF networks reduces to the mean-field solution with infinite-range interactions; however, it is revealed [2–4] that various properties such as phase diagrams and critical exponents depend on the degree exponent λ. Accordingly, the critical behavior of SG models on SF networks is physically much richer than the mean-field solutions.

In SG models, to obtain the free energy, one needs take an average over quenched disorder, such as coupling strengths. To facilitate the calculations of such an ensemble average, the replica method is prototypically used as $-\beta F = \langle \ln Z \rangle_\xi = \lim_{n\to 0}[\langle Z^n \rangle_\xi - 1]/n$, where $\beta = 1/T$, F, and Z represent the free energy and the partition function, respectively, and ξ represents the coupling strength. The n-th power of the partition function $\langle Z^n \rangle_\xi$ indicates the partition functions of n replicas. Even though n replicas have to be totally independent of each other, a so-called replica-symmetry breaking phase can exist, which is not a generic feature of the SG model but an artifact of the replica method. To avoid this undesirable product, van Hemmen [5] introduced a new method using a quenched random exchange coupling strength, which could provide an analytic solution without replicas. The phase diagram he obtained for the Ising spin SG model with long-range interactions was different from that obtained from the replica method. On the other hand, the SG model on SF networks has been investigated analytically using the replica method [3, 4]. Thus, as it is complementary to our previous work, in this paper, we analytically investigate the van Hemmen SG (vHSG) model on SF networks.

The main results of this paper are as follows: We find that the four different phases, paramagnetic (P), ferromagnetic (F), mixed phase (M), and SG appear in the phase diagram. Even though this feature was also obtained using the replica method [3], the phase diagrams obtained here using the van Hemmen's method differ from each other. In this method, the M phase can appear in the lower temperature region than the temperature region of the SG phase. For finite $\lambda > 3$, the phase boundaries are deformed but all the phases exist. However, for $2 < \lambda < 3$, the P phase disappears and the SG phase exists only at $J_0 = 0$. One of the distinct features of the vHSG model is the occurrence of a first-order transition curve and a critical endpoint (CE) at which the second-

* dohyunkim@sogang.ac.kr
† bkahng@snu.ac.kr

order transition curve terminates in the first-order transition curve. At the CE, a hybrid phase transition occurs in which properties of the second-order and first-order transitions emerge simultaneously. This feature does not occur in the SG model with replicas. The exponent of the SG order parameter is different from that obtained from the replica method.

The paper is organized as follows: in Section II, the static model for generating SF networks is introduced. In Section III, we obtain the free energy of the vHSG model on the static SF networks. In Section IV, we analytically obtain phase boundaries among the P, F, M and SG phases for various conditions of temperature T, ferromagnetic coupling strength J_0 in units of J, degree exponent λ, and mean degree K. In Section V, we generate several phase diagrams under various conditions of T, J_0, λ and K. These phase diagrams represent peculiar characteristics of the vHSG model showing the CE and hybrid phase transition. In Section VI, we show that the exponent for the SG order parameter is different from that obtained from the replica method. In Section VII, we conclude our investigations about the vHSG model on the static SF networks.

II. THE STATIC MODEL FOR SF NETWORKS

We use the static model to generate SF networks, which enable us to obtain various physical properties of the vHSG model analytically. The static model is defined as follows: N nodes are present in a system from the beginning. Each node i ($i = 1, 2, \ldots, N$) is assigned a weight p_i. A pair of nodes (i, j) is chosen with probabilities p_i and p_j, respectively, and they are connected with a link, unless the pair is already connected. This process is repeated $NK/2$ times. Then, the resulting network gets mean degree K. In such weighted random networks, the probability that a given pair of nodes (i, j) ($i \neq j$) is connected, denoted as f_{ij}, is given as $f_{ij} = 1 - \exp(-NKp_ip_j)$. Depending on a given function p_i, various types of network structures are generated. First, when $p_i = 1/N$ is given, independent of the index i, the resulting network is reduced to a random network introduced by an Erdős-Rényi (ER) graph [6, 7]. The probability that nodes i and j are connected during the $NK/2$ trials is given by $f_{ij} \approx K/N$. Second, when p_i is given as

$$p_i = \frac{i^{-\mu}}{\zeta_N(\mu)} \tag{1}$$

where μ is a control parameter in the range $[0, 1)$, $\zeta_N(\mu) \equiv \sum_{j=1}^{N} j^{-\mu} \approx N^{1-\mu}/(1-\mu)$, and an SF network is generated following a power-law degree distribution $P_d(k) \sim k^{-\lambda}$ with $\lambda = 1 + 1/\mu$ [3, 4, 8, 9]. Next, when $K = N$, a fully connected network is generated, which contains infinite-range interactions. We remark that the previous study by van Hemmen was limited to the extreme case $K = N$ [5].

III. THE VHSG MODEL WITHOUT REPLICAS

The Hamiltonian of the vHSG model on a graph G is given as

$$\mathcal{H} = -\sum_{(i,j)\in G} J_{ij} S_i S_j \quad (S_i = \pm 1), \tag{2}$$

where J_{ij} is nonzero when the nodes i and j are connected in G. The graph is generated with the weight set $\{p_i\}$ in Eq. (1). The probability of G in the quenched (i.e., we assume that once a connection between two nodes is fixed, it will not be changed forever) random network ensemble is defined as

$$P_K(G) = \prod_{(i,j)\in G} f_{ij} \prod_{(i,j)\notin G} (1 - f_{ij}) \tag{3}$$

with $f_{ij} = 1 - \exp(-NKp_ip_j)$, p_i being given in Eq.(1). Then, the ensemble average over graph configurations for a given physical quantity A is taken as

$$\langle A \rangle_K = \sum_G P_K(G) A(G), \tag{4}$$

where $\langle \cdots \rangle_K$ denotes the average over different graph configurations.

In the SG problem, the coupling strengths $\{J_{ij}\}$ are also quenched random variables. The quenched random exchange interaction variable J_{ij} is given as

$$J_{ij} = \frac{1}{2}\big[J(\xi_i\eta_j + \xi_j\eta_i) + J_0\big], \tag{5}$$

where ξ_i and η_i are independent and randomly distributed variables with even distributions around zero and finite variance, and J and J_0 are positive constants. In our model, J_{ij} can be positive or negative, thus such ferromagnetic and antiferromagnetic bonds induce frustration, an ingredient of a SG model. After taking an ensemble average over the randomness of $\{\xi_i, \eta_i\}$, a given physical quantity A is obtained as

$$\langle A \rangle_{\xi,\eta} = \int \prod_i d\xi_i d\eta_i P(\xi_i) P(\eta_i) A(\{\xi_i\}, \{\eta_i\}), \tag{6}$$

where $\langle \cdots \rangle_{\xi,\eta}$ is an average over the quenched disorder of the ξ_i and η_i. Thus, the free energy F is evaluated as $-\beta F = \langle \langle \ln Z \rangle_{\xi,\eta} \rangle_K$, where Z ($\equiv \mathrm{Tr}\ \exp\{-\beta\mathcal{H}\}$) is the partition function for a given distribution of $\{\xi_i\}$ and $\{\eta_i\}$ on a particular graph G with inverse temperature $\beta = 1/T$.

The analytic solutions of the original version of the vHSG model could be derived without using the replica method [5]. Although we consider not only the average over the quenched disorder of ξ_i and η_i but also the

average over different graph configurations, we find that $\langle\langle \ln Z\rangle_{\xi,\eta}\rangle_K$ can be obtained on SF networks without the replica method. For this, we use the Taylor expansion of the natural logarithmic function:

$$\ln Z = (Z-1) - \frac{1}{2}(Z-1)^2 + \frac{1}{3}(Z-1)^3 - \cdots . \quad (7)$$

Let us first calculate $\langle\langle Z-1\rangle_{\xi,\eta}\rangle_K$ as follows:

$$\begin{aligned}\langle\langle Z-1\rangle_{\xi,\eta}\rangle_K &= \Big\langle\Big\langle \mathop{\rm Tr}_{\{S_i=\pm1\}} \exp\Big(\beta\sum_{(i,j)\in G} J_{ij}S_iS_j\Big) - 1\Big\rangle_{\xi,\eta}\Big\rangle_K \\ &= \mathop{\rm Tr}_{\{S_i=\pm1\}} \exp\Big[\sum_{(i,j)} \ln\Big\{1 + f_{ij}\Big(\Big\langle \exp\left(\beta J_{ij}S_iS_j\right)\Big\rangle_{\xi,\eta} - 1\Big)\Big\}\Big] - 1 \\ &= \mathop{\rm Tr}_{\{S_i=\pm1\}} \exp\Big[\sum_{(i,j)} f_{ij}\Big\langle \beta J_{ij}S_iS_j + \frac{1}{2!}(\beta J_{ij}S_iS_j)^2 + \frac{1}{3!}(\beta J_{ij}S_iS_j)^3 + \cdots\Big\rangle_{\xi,\eta}\Big] - 1. \end{aligned} \quad (8)$$

Inside $[\cdots]$ of the last formula of Eq. (8), the second term containing $(S_iS_j)^2$ is a function which does not depend on S_i so that it can be neglected. The third term inside $[\cdots]$ has both 1/3! and $(J_{ij})^3 \sim (1/2)^3$ so it becomes very small compared with the first term. Furthermore, $(Z-1)^2$ and other terms in Eq. (7) can also be neglected because they contain a higher order of $f_{ij}(<1)$. Therefore, to obtain $\langle\langle \ln Z\rangle_{\xi,\eta}\rangle_K$, it may be sufficient to consider only the first term of Eq. (8) within the leading order of f_{ij}.

Using the definition of J_{ij}, the first term inside $[\cdots]$ of Eq. (8) becomes

$$\begin{aligned}\sum_{(i,j)} f_{ij}\beta J_{ij}S_iS_j &= \sum_{(i,j)} \frac{1}{2}NK\beta\big[J(\xi_i\eta_j + \xi_j\eta_i) + J_0\big](p_iS_i)(p_jS_j) \\ &= \frac{1}{2}NK\beta J\Big[\Big(\sum_i p_i(\xi_i+\eta_i)S_i\Big)^2 - \Big(\sum_i p_i\xi_iS_i\Big)^2 - \Big(\sum_i p_i\eta_iS_i\Big)^2\Big] + \frac{1}{2}NK\beta J_0\Big(\sum_i p_iS_i\Big)^2 + C, \end{aligned} \quad (9)$$

where C is independent of S_i.

Now $\left(\sum_i p_i(\xi_i+\eta_i)S_i\right)^2$, $\left(\sum_i p_i\xi_iS_i\right)^2$, $\left(\sum_i p_i\eta_iS_i\right)^2$, and $\left(\sum_i p_iS_i\right)^2$ can be simplified using the Hubbard-Stratonovich transformation,

$$\exp\Big\{\frac{1}{2}\lambda a^2\Big\} = \sqrt{\frac{\lambda}{2\pi}}\int_{-\infty}^{\infty} dx\ \exp\Big\{-\frac{1}{2}\lambda x^2 + \lambda a x\Big\}\ . \quad (10)$$

Therefore, we obtain

$$\begin{aligned}\langle\langle \ln Z\rangle_{\xi,\eta}\rangle_K &= \left(\frac{NK\beta J}{2\pi}\right)^{3/2}\left(\frac{NK\beta J_0}{2\pi}\right)^{1/2}\int_{-\infty}^{\infty} dxdydzdw\ \exp\Big[-\frac{1}{2}NK\beta J(x^2-y^2-z^2)\Big]\cdot\exp\Big[-\frac{1}{2}NK\beta J_0w^2\Big] \\ &\quad\times \mathop{\rm Tr}_{\{S_i=\pm1\}}\Big\langle \exp\Big[NK\beta J\sum_i\Big\{xp_i(\xi_i+\eta_i)S_i - yp_i\xi_iS_i - zp_i\eta_iS_i\Big\}\Big]\exp\Big[NK\beta J_0w\Big(\sum_i p_iS_i\Big)\Big]\Big\rangle_{\xi,\eta} - 1 \\ &= \left(\frac{NK\beta J}{2\pi}\right)^{3/2}\left(\frac{NK\beta J_0}{2\pi}\right)^{1/2}\int_{-\infty}^{\infty} dx\ dy\ dz\ dw\ \Big\langle \exp[-NG(x,y,z,w)]\Big\rangle_{\xi,\eta} - 1 \end{aligned} \quad (11)$$

where

$$G(x,y,z,w) \equiv \frac{1}{2}K\beta J(x^2-y^2-z^2) + \frac{1}{2}K\beta J_0w^2 - \frac{1}{N}\sum_i \ln \mathop{\rm Tr}_{\{S_i=\pm1\}}\exp(\beta\tilde{\mathcal{H}}_i) \quad (12)$$

with the effective Hamiltonian

$$\tilde{\mathcal{H}}_i \equiv NKJ(x-y)p_i\xi_iS_i + NKJ(x-z)p_i\eta_iS_i + NKJ_0wp_iS_i. \quad (13)$$

In the thermodynamic limit ($N\to\infty$), the free energy f per node can be obtained using the steepest descent

method as

$$\beta f = \min\Big\langle \frac{1}{2}K\beta J\big\{(q_1+q_2)^2 - q_1^2 - q_2^2\big\} + \frac{1}{2}K\beta J_0 m^2 - \frac{1}{N}\sum_i \ln \operatorname*{Tr}_{\{S_i=\pm 1\}} \exp(\beta\tilde{\mathcal{H}}_i')\Big\rangle_{\xi,\eta} \quad (14)$$

with

$$\tilde{\mathcal{H}}_i' \equiv NKJp_i(q_2\xi_i + q_1\eta_i)S_i + NKJ_0 m p_i S_i. \quad (15)$$

Here, three order parameters are defined as follows:

$$\begin{aligned} q_1 &\equiv \sum_i p_i \langle \xi_i S_i\rangle_i \\ q_2 &\equiv \sum_i p_i \langle \eta_i S_i\rangle_i \\ m &\equiv \sum_i p_i \langle S_i\rangle_i \end{aligned} \quad (16)$$

where $q_{1(2)}$ and m represent spin glass order parameters and magnetization, respectively, and $\langle\cdots\rangle$ represents $\langle A\rangle_i \equiv \mathrm{Tr}\,[A\, e^{\beta\tilde{\mathcal{H}}_i'}]/\mathrm{Tr}\, e^{\beta\tilde{\mathcal{H}}_i'}$.

The free energy f per node becomes minimum when we take $q_1 = q_2 = q$ as

$$\beta f = K\beta J q^2 + \frac{1}{2}K\beta J_0 m^2 - \frac{1}{N}\sum_i \Big\langle \ln\big(2\cosh\Theta_i\big)\Big\rangle_{\xi,\eta} \quad (17)$$

with $\Theta_i \equiv NK\beta p_i\big[J(\xi_i+\eta_i)q + J_0 m\big]$.

We determine m and q by the condition that f resumes the stable extrema and obtain the self-consistency equations of m and q (i.e., $\partial f/\partial m = \partial f/\partial q = 0$):

$$m = \Big\langle \sum_i p_i \tanh\Theta_i\Big\rangle_{\xi,\eta} \quad (18)$$

and

$$q = \Big\langle \sum_i p_i\Big(\frac{\xi_i+\eta_i}{2}\Big)\tanh\Theta_i\Big\rangle_{\xi,\eta}. \quad (19)$$

Now we restrict ourselves to the case of discrete (or bimodal) distribution of ξ and η:

$$P(\xi_i) = \frac{1}{2}\delta(\xi_i - 1) + \frac{1}{2}\delta(\xi_i + 1) \quad (20)$$

$$P(\eta_i) = \frac{1}{2}\delta(\eta_i - 1) + \frac{1}{2}\delta(\eta_i + 1). \quad (21)$$

Then, m, q, and f are given by

$$\begin{aligned} m &= \Big\langle \sum_i p_i \tanh\Theta_i\Big\rangle_{\xi,\eta} \quad (22)\\ &= \int \prod_i d\xi_i d\eta_i P(\xi_i)P(\eta_i) \sum_i p_i \tanh\Theta_i \\ &= \sum_i \frac{p_i}{4}\Big[\tanh(\Theta_{i++}) + 2\tanh(\Theta_{i+-}) + \tanh(\Theta_{i--})\Big], \\ q &= \Big\langle \sum_i p_i\Big(\frac{\xi_i+\eta_i}{2}\Big)\tanh\Theta_i\Big\rangle_{\xi,\eta} \quad (23)\\ &= \int \prod_i d\xi_i d\eta_i P(\xi_i)P(\eta_i) \sum_i p_i\Big(\frac{\xi_i+\eta_i}{2}\Big)\tanh\Theta_i \\ &= \sum_i \frac{p_i}{4}\Big[\tanh(\Theta_{i++}) - \tanh(\Theta_{i--})\Big], \end{aligned}$$

and

$$f = KJq^2 + \frac{1}{2}KJ_0 m^2 - \frac{T}{4N}\sum_i \Big[\ln\big(2\cosh\Theta_{i++}\big) + 2\ln\big(2\cosh\Theta_{i+-}\big) + \ln\big(2\cosh\Theta_{i--}\big)\Big], \quad (24)$$

where

$$\begin{aligned} \Theta_{i++} &= NK\beta p_i(2Jq + J_0 m) \\ \Theta_{i+-} &= NK\beta p_i J_0 m \\ \Theta_{i--} &= NK\beta p_i(-2Jq + J_0 m). \end{aligned} \quad (25)$$

Therefore, m has a value in the range [0,1], whereas q has a value in [0,1/2]. In particular, at $T = 0$, $\{m, q\}$ has only two solutions: $\{1, 0\}$ and $\{1/2, 1/2\}$.

IV. THE PHASE BOUNDARIES

We define the four phases for the bimodal distributions of ξ and η in Eqs. (20) and (21) as follows: the P phase with $m = q = 0$; the F phase with $m > 0$ but $q = 0$; the SG phase with $m = 0$ but $q > 0$; and the M phase with $m > 0$ and $q > 0$. We obtain several phase diagrams in the $T/J - \lambda$ plane, in the $T/J - K$ plane, and in the $T/J - J_0/J$ plane. The phase boundary can be obtained from the self-consistency equations for m and q in Eqs. (22) and (23).

A. At the edge of $q = 0$

The P-SG and F-M phase boundaries can be obtained by taking the derivative of Eq. (22) and by taking the limit $q \to 0$, the edges of the SG and the M phases as follows:

$$T/J = KN\sum_{i=1}^{N} p_i^2\, \mathrm{sech}^2\big(NKp_i m J_0/T\big). \quad (26)$$

1. The P-SG phase boundary

The P-SG phase boundary is determined by Eq. (26) after taking the limit $m \to 0$, which determines the SG transition temperature T_g,

$$T_g/J = KN \sum_{i=1}^{N} p_i^2 \equiv K/K_p, \tag{27}$$

where

$$\frac{1}{K_p} = N \sum_{i=1}^{N} p_i^2 \overset{N\to\infty}{\longrightarrow} \frac{(\lambda-2)^2}{(\lambda-1)(\lambda-3)} \tag{28}$$

becomes infinite as $\lambda \to 3.0^+$ and one as $\lambda \to \infty$ [3]. The SG temperature T_g/J is linear with respect to K with a slope $1/K_p$. The slope increases from one to infinite as λ is decreased from infinity to 3.0^+. Therefore, for $2 < \lambda \leq 3$, there exists only the SG phase for $K > 0$.

2. The F-M phase boundary

To obtain the F-M boundary, we first consider the $T = 0$ case. In this case, the free energy is obtained as

$$f_{T=0} = K(Jq^2 + \frac{1}{2}J_0 m^2). \tag{29}$$

As we previously obtained at $T = 0$, there exist two solutions $\{m, q\} = \{1, 0\}$ and $\{1/2, 1/2\}$, which represent the states of the F and M phases, respectively. To determine which state is more stable between the two solutions, we compare the free energy of each of the two states: i) $f_{T=0}|_M = f_{T=0}(m = 1/2, q = 1/2) = K(J/4 + J_0/8)$ and ii) $f_{T=0}|_F = f_{T=0}(m = 1, q = 0) = KJ_0/2$. Thus, when $J_0/J = 2/3$, the two free energies become the same in their magnitudes, and thus $J_0/J = 2/3$ becomes the M-F phase boundary at $T = 0$. When $f_{T=0}|_M < f_{T=0}|_{FM}$, i.e., $J_0/J < 2/3$, the M phase is stable at $T = 0$, and vice versa. This solution is consistent with the previous one obtained in Ref. [5] on fully connected networks. Actually the point $(J_0/J, T/J) = (2/3, 0)$ becomes a critical point (CP) at $T = 0$, which is invariant regardless of λ, as will be discussed later.

Next, let us consider the F-M boundary at finite temperature. We rewrite Eq. (26) using Eq. (1) as follows:

$$T/J = K(1-\mu)^2 N^{-1} \sum_{i=1}^{N} (N/i)^{2\mu} \operatorname{sech}^2\big((N/i)^{\mu} K(1-\mu) m J_0/T\big). \tag{30}$$

For $\lambda \to \infty$ (ER case), i.e., $\mu = 0$,

$$T/J = K \operatorname{sech}^2\big(KmJ_0/T\big). \tag{31}$$

For finite $\lambda > 2$, i.e., $0 < \mu < 1$, under the condition $J_0/J < 1.0$, T/J becomes zero in the thermodynamic limit ($N \to \infty$). For $\lambda > 3$, i.e., $0 \leq \mu < 1/2$, with $J_0/J = 1.0$, the right-hand side of Eq. (30) depends on $\sum_{i=1}^{N} i^{-2\mu}$ so that T/J becomes infinite in the limit $N \to \infty$. For $2 < \lambda \leq 3$, i.e., $1/2 \leq \mu < 1$, with $J_0/J = 1.0$, the right-hand side of Eq. (30) depends on $N^{2\mu-1}$ so that T/J becomes infinite in the limit $N \to \infty$.

B. At the edge of $m = 0$

The P-F and SG-M phase boundaries can be determined by taking derivative of Eq. (23) and by taking the limit $m \to 0$, the edges of the F and the M phases, as follows:

$$T/J = \frac{1}{2}(J_0/J)KN \sum_{i=1}^{N} p_i^2 \Big[1 + \operatorname{sech}^2\big(2NKp_i qJ/T\big)\Big]. \tag{32}$$

1. The P-F phase boundary

The P-F phase boundary, which is located at $J_0/J \geq 1.0$, is determined by setting $q = 0$ in Eq. (32). Since $\operatorname{sech}(0) = 1$, the transition temperature T_c is obtained for $J_0/J \geq 1.0$ as

$$T_c/J = (J_0/J)KN \sum_{i=1}^{N} p_i^2 = (J_0/J)(K/K_p). \tag{33}$$

When λ approaches 3.0^+, the slope $(1/K_p)$ of the P-F boundary becomes infinite in the $T/J - J_0/J$ plane.

2. The SG-M phase boundary

Since $\operatorname{sech}(\infty) = 0$, the SG-M boundary in the limit $N \to \infty$ simply becomes as follows:

$$T/J = \frac{1}{2}(J_0/J)KN \sum_{i=1}^{N} p_i^2 = \frac{1}{2}(J_0/J)(K/K_p), \tag{34}$$

which is a half of T_c, the transition temperature between P and F phases.

C. At the edge of $m = 0$ and $q = 0$

The first-order SG-F phase boundary in the $T/J-J_0/J$ plane is determined as the intersection of the two phase boundaries given by Eqs. (26) and (32):

$$J_0/J = \frac{2\sum_{i=1}^{N} i^{-2\mu}\ \mathrm{sech}^2\left((N/i)^{\mu}K(1-\mu)mJ_0/T\right)}{\sum_{i=1}^{N} i^{-2\mu}\ \left[1+\mathrm{sech}^2\left(2(N/i)^{\mu}K(1-\mu)qJ/T\right)\right]}. \tag{35}$$

For $\lambda \to \infty$ (ER case), i.e., $\mu = 0$,

$$J_0/J = \frac{2\ \mathrm{sech}^2\left(KmJ_0/T\right)}{1+\mathrm{sech}^2\left(2KqJ/T\right)}. \tag{36}$$

For finite $\lambda > 2$, i.e., $0 < \mu < 1$, $J_0/J = 1.0$ in the limit $N \to \infty$.

V. PHASE DIAGRAM

Fig. 1(a) and (b) show the phase diagram in the $T/J-K$ plane at $J_0 = 0$ for the case $\lambda > 3$ and $2 < \lambda \leq 3$, respectively. The P-SG phase boundary can be determined by Eq.(27). For the ER case ($\lambda \to \infty$), $p_i = 1/N$, i.e., $K_p = 1$; thus, the slope of the P-SG boundary becomes one. As λ is decreased, according to Eq.(28), the slope of P-SG boundary becomes steeper and eventually it becomes infinite at $\lambda = 3$. Therefore, for $2 < \lambda \leq 3$, there exists only the SG phase for nonzero K, as shown in Fig. 1(b).

Fig. 2 shows the phase diagram at $J_0/J = 0$ for three values of K in the $T/J - \lambda$ plane. Following Eq. (27), as λ is increased, the P-SG boundary, (which is the SG transition temperature T_g), tends to be independent of λ and its value becomes proportional to K. As $\lambda \to 3^+$, T_g increases drastically. We note that there exists only the SG phase for $2 < \lambda \leq 3$ in the limit $N \to \infty$.

Figs. 3 show the phase diagrams in the $T/J - \lambda$ plane for several values of J_0/J. The phase boundaries are determined by Eqs. (27), (33) and (34). When $0 < J_0 < 2/3$ in (a), not only the P and SG phases exist for $\lambda > 3$, but also the M phase appears in the region $2 < \lambda \leq 3$ and below the SG phase as T is lowered for $\lambda > 3$. When $2/3 \leq J_0 \leq 1$ in (b), the F phase exists in the region $2 < \lambda \leq 3$ and the P, SG, and M phases appear for $\lambda > 3$ as they do in the way of (a). When $J_0 > 1$ in (c), the F phase exists for $2 < \lambda \leq 3$ and below the P phase as T is lowered.

Figs. 4 show the phase diagrams in the $T/J - J_0/J$ plane in the thermodynamic limit (a) for the ER case, (b) for $\lambda > 3$, and (c) for $2 < \lambda \leq 3$. Five phase boundaries appear among the four phases, which are determined by Eqs.(27), (30), (33), (34), and (35). Moreover, three different types of singular points exist: critical point (CP), critical endpoint (CE), and multicritical point (MCP). At $T = 0$, the M-F phase transition occurs at the CP $J_0/J = 2/3$, which is second-order. In (a), the F-M and SG-F transitions are first-order, which is determined by Eq. (31) and (36), respectively. The first-order transition curve between the F and M phases runs from the CP to the CE [10, 11], at which the transition changes

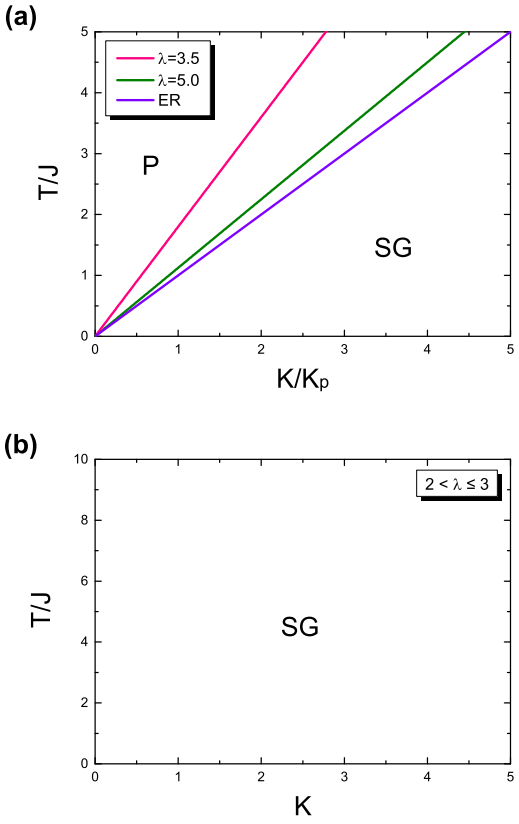

FIG. 1. (Color online) Phase diagram in the $T/J - K$ plane when $J_0 = 0$ for the cases (a) $\lambda > 3$ and (b) $2 < \lambda \leq 3$. P and SG phases exist in (a) and only SG phase exists in (b).

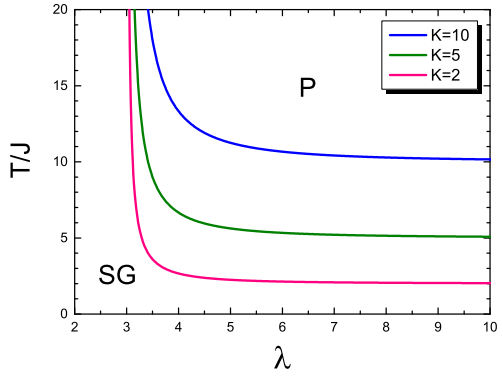

FIG. 2. (Color online) Phase diagram in the $T/J - \lambda$ plane when $J_0/J = 0$ for three different values of K ($K = 2, 5$ and 10). The SG transition temperature normalized by J T_g/J is the P-SG phase boundary, which depends on λ, but becomes constant K in the limit $\lambda \to \infty$.

to a hybrid phase transition, which exhibits properties of the second-order and the first-order transitions simultaneously [12–16]. As T is increased, beyond the CE, the first-order transition curve sustains until it meets a MCP. At this point, the first-order transition curve meets the two second-order transition curves and the three phases P, SG, and F merge, and a second-order transition occurs.

When $3 < \lambda < \infty$ in (b), the F-M boundary at zero temperature locates on the line $2/3 \le J_0/J \le 1.0$ and forms a vertical straight line at $J_0/J = 1$ spanning from $T = 0$ to the CE. The SG-F boundary also forms a vertical straight line from the CE to the MCP at $J_0/J = 1.0$. Therefore, the CP, CE and MCP locate at $(2/3, 0)$, $(1.0, K/2K_p)$, and $(1.0, K/K_p)$ in the T/J-J_0/J plane, respectively. Such a drastic change of the first-order transition curve from the ER case to the finite-λ case can be observed only in the thermodynamic limit. However, for finite systems, as shown in Fig. 5(a) and (b) below, there exists no such a drastic change.

For $2 < \lambda \le 3$ in (c), the slope of the SG-M phase boundary becomes infinite so that the M phase covers the region $0 < J_0/J < 2/3$ in the entire range of temperature. Furthermore, since both the M-F and SF-F phase boundaries are vertical lines and the former line locates at $J_0/J = 2/3$, the F phase covers all the temperature range in the region $J_0/J > 2/3$ as shown in (c).

Figs. 5 show the phase diagrams in the $T/J - J_0/J$ plane for finite systems with $N = 1000$ and $K = 5$. As in Fig. 4, the five different phase boundaries and the three singular points exist. The phase boundaries are determined by Eqs. (28), (30), (32), (33), and (34) with $N = 1000$. For the ER case (a), the phase diagram for infinite systems remains the same even for finite systems, because the analytic solutions for the ER case are independent of system sizes. In (b), as λ is decreased, the F-M boundary deforms slightly from the one in (a).

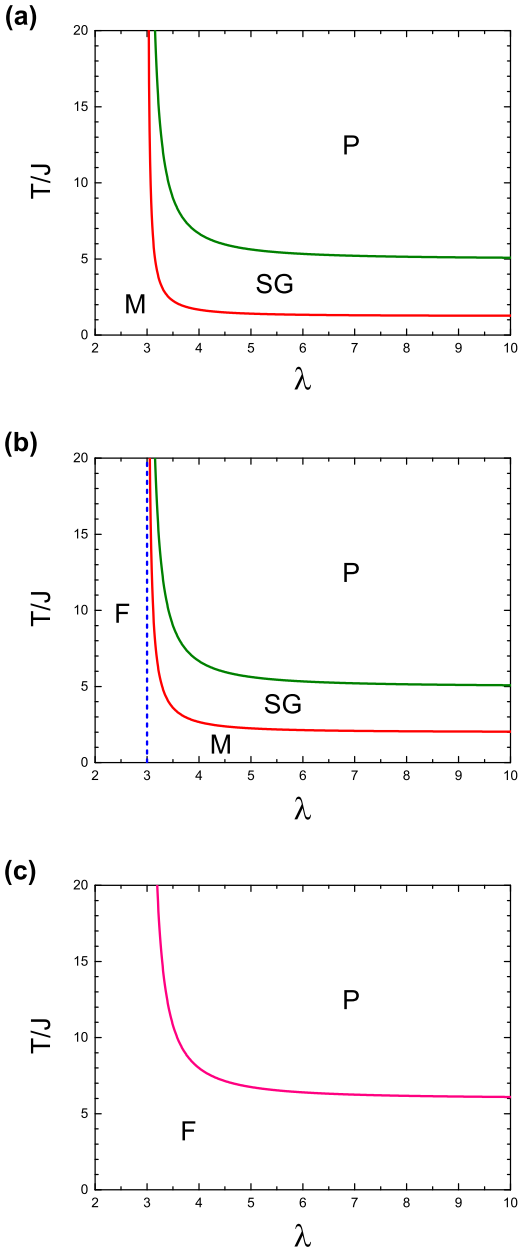

FIG. 3. (Color online) Phase diagram in the $T/J - \lambda$ plane for finite $J_0 > 0$: (a) $J_0/J = 0.5$, (b) $J_0/J = 0.8$, and (c) $J_0/J = 1.2$. K is fixed as $K = 5$. (a) For $0 < J_0/J < 2/3$, the M phase appears in the region $2 < \lambda \le 3$ and below the SG phase as T is lowered for $\lambda > 3$. (b) For $2/3 \le J_0/J \le 1$, the F phase appears in the region $2 < \lambda \le 3$, but for $\lambda > 3$, the M phase still exists below the SG phase as T is lowered. Thus, for $\lambda > 3$, as T is lowered from sufficiently high temperature, successive phase transitions occur following the order P $\to$ SG $\to$ M. (c) For $J_0/J > 1$, there exists only the F phase for $2 < \lambda \le 3$. For $\lambda > 3$, the F phase also exists below the P phase as T is lowered.

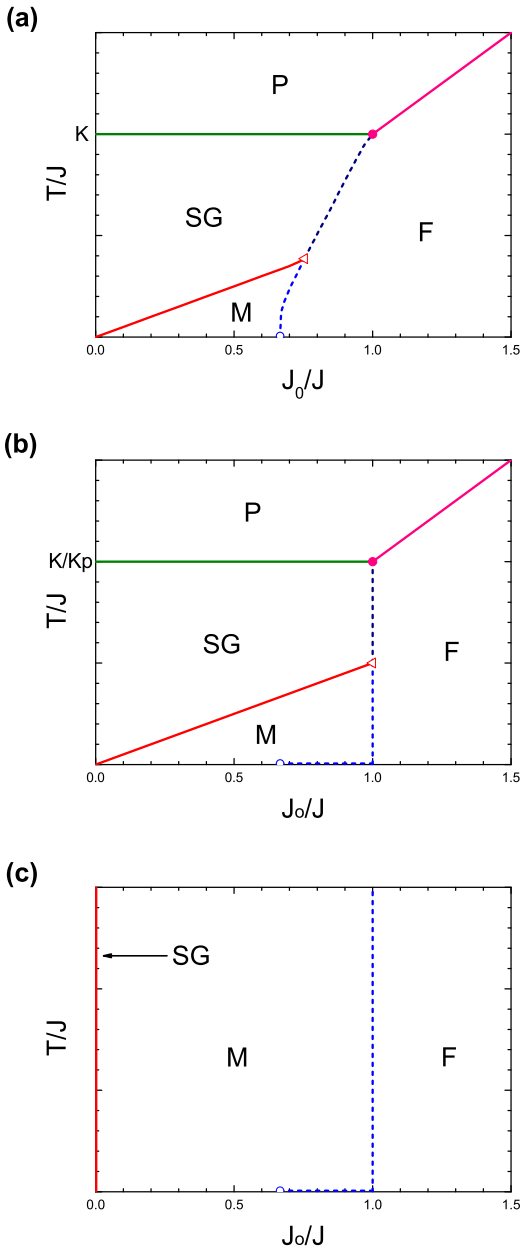

FIG. 4. (Color online) Phase diagram in the $T/J - J_0/J$ plane in the limit $N \to \infty$ (a) for the ER case ($\lambda \to \infty$), (b) for $\lambda > 3$ and (c) for $2 < \lambda \leq 3$. The solid-line (dotted-line) indicates the second-order (first-order) phase transition. Dots denoted by $\circ, \triangleleft, \bullet$ represent the critical point, critical endpoint, and multicritical point, respectively.

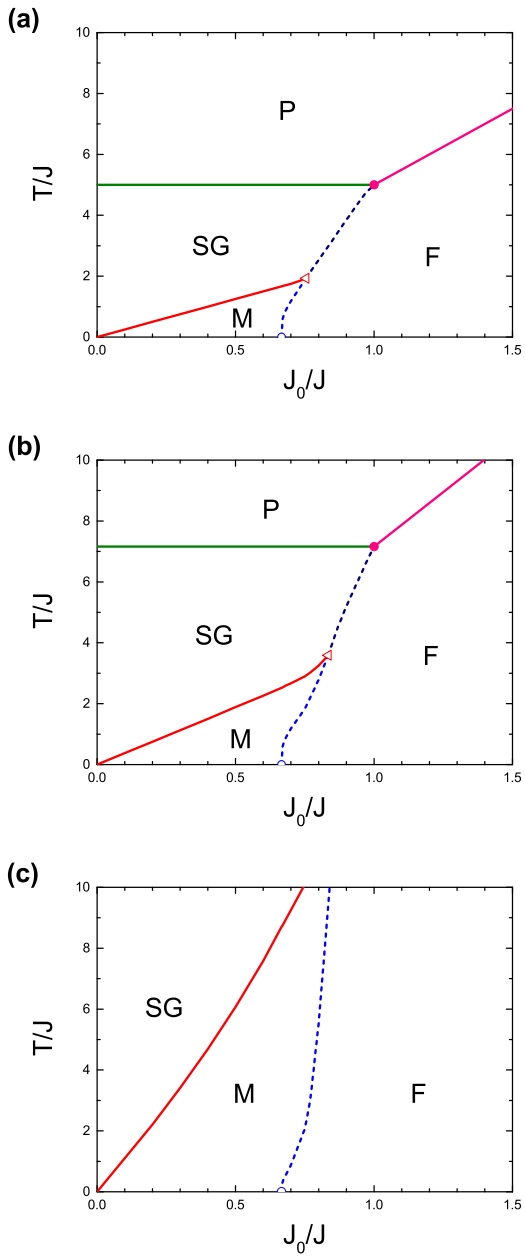

FIG. 5. (Color online) Phase diagram in the $T/J - J_0/J$ plane in finite systems with $N = 1000$ and $K = 5$ (a) for the ER case ($\lambda \to \infty$), (b) for $\lambda = 3.5$ and (c) for $\lambda = 2.5$. The solid line (dotted line) indicates the second-order (first-order) phase transition. Dots denoted by $\circ, \triangleleft, \bullet$ represent critical point, critical endpoint, and multicritical point, respectively.

The same applies for the SG-F phase boundary. The CP remains at the same point. The CE and MCP still exist, but move to higher temperature positions as λ is decreased.

For $2 < \lambda \leq 3$, the P-SG and P-F boundaries move in the higher temperature region. As a result, the SG-M and M-F boundaries become much steeper and the regions of SG, M, and F phases become extended, as shown in Fig. 5(c).

We remark that the positions of the CP and MCP are fixed as $(J_0/J, T/J) = (2/3, 0)$ and $(1.0, K/K_p)$, independent of N, but the CE depends on N. Let us denote the coupling strength J_0 at the CE for a given J as $J_{0,\mathrm{CE}}(N)$. For $J_{0,\mathrm{CE}}(N) < J_0/J < 1.0$, when T is lowered from sufficient high temperature, the SG order parameter increases continuously from zero to finite $q(T)$

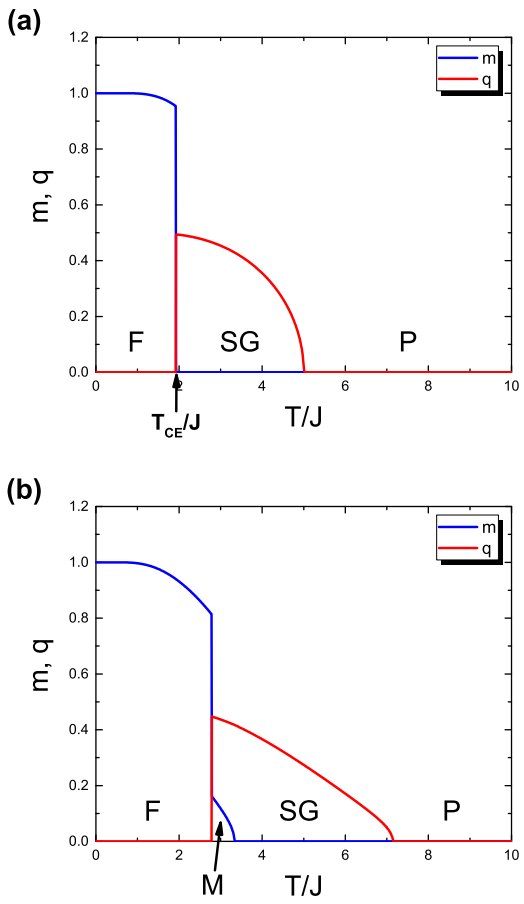

FIG. 6. (Color online) Plot of the order parameters m and q versus T/J (a) for the ER case ($\lambda \to \infty$) with $J_0/J = 0.754$, and (b) for $\lambda = 3.5$ with $J_0/J = 0.800$. Data are obtained from the systems with $N = 1000$ and $K = 5.0$. As T is lowered from a sufficiently high temperature, the order parameter m jumps suddenly at T_c and continuously increases below T_c following the second-order transition pattern. However, the SG order parameter increases continuously from T_g but drops suddenly at T_c.

at T_g. As T is lowered even further to T_c, $q(T)$ drops suddenly to zero, however, the ferromagnetic order parameter $m(T)$ jumps suddenly from zero to $m(T_c)$. When T is lowered beyond T_c, $m(T)$ increases continuously following a pattern of the second-order phase transition. Thus, the order parameter $m(T_c)$ exhibits the natures of the second-order and the first-order phase transitions. Thus, the phase transition at the CE is hybrid. The behaviors of the order parameters m and q are shown in Fig. 6(a). At the CE, as temperature is lowered, m jumps from zero to nonzero; however, q becomes zero from nonzero.

For $2/3 < J_0/J < J_{0,\mathrm{CE}}(N)/J$, when T is lowered from a sufficiently high temperature, the SG order parameter increases continuously from zero to finite $q(T)$ at T_g. As T is lowered across the SG-M boundary, $q(T)$ still increases continuously and $m(T)$ begins to increase from zero continuously. When T is lowered to the M-F boundary, $m(T)$ jumps suddenly from a finite value to $m(T_c)$; however, $q(T)$ suddenly drops to zero. The behaviors of the order parameters m and q are shown in Fig. 6(b).

The CE for the ER case ($\lambda \to \infty$) with $N = 1000$ and $K = 5.0$ is located at $(J_0/J, T/J) = (0.754, 1.931)$ as shown in Fig. 5(a). Meanwhile, the CE for $\lambda = 3.5$ under the same N and K is located at $(J_0/J, T/J) = (0.835, 3.590)$ as shown in Fig. 5(b).

VI. THE SG ORDER PARAMETER

In the SG phase ($m = 0$, $q \neq 0$), the SG order parameter q is determined by the self-consistency equation,

$$q = \frac{1}{2}\sum_i p_i \tanh(2NKp_iJq/T). \tag{37}$$

Now, we determine the critical behavior of q near the SG transition T_g. The right hand side of Eq. (37) contains a sum of the type

$$S(y) = \frac{1}{N}\sum_i H(Np_iy/(1-\mu)), \tag{38}$$

where $y = (1-\mu)2KqJ/T$ and $H(x) = x\tanh x$. When y is small, q can be expanded following the method used in Appendix B of Ref. [3] as

$$q = A(\lambda)T^{2-\lambda}q^{\lambda-2} + J\frac{K}{K_p}T^{-1}q + B(\lambda)K^2T^{-2}q^2 + \mathcal{O}(q^3), \tag{39}$$

where $A(\lambda)$ and $B(\lambda)$ are λ-dependent positive coefficients.

Therefore, we obtain that

$$q \sim \begin{cases} T^{-(\lambda-2)/(3-\lambda)} & \text{for} \quad 2 < \lambda < 3, \\ T\exp(-T/KJ) & \text{for} \quad \lambda = 3, \\ \epsilon_g^{1/(\lambda-3)} & \text{for} \quad 3 < \lambda < 4, \\ \epsilon_g/\ln\epsilon_g^{-1} & \text{for} \quad \lambda = 4, \\ \epsilon_g & \text{for} \quad \lambda > 4, \end{cases} \tag{40}$$

where T is presumed to be extremely high for $2 < \lambda < 3$ and $\epsilon_g \equiv (T_g - T)/T_g \to 0$ for $\lambda > 3$. We remark that the critical exponent of q for $2 < \lambda < 3$ is a half of that obtained using the replica trick [3], because the self-consistency equation q of the vHSG model is in the form of tanh instead of $\tanh^2$, the form of the SG model with replicas.

VII. CONCLUSION

In summary, we have analytically investigated the phase diagram and the transition behavior of the van Hammen SG model on the static SF networks without replicas (method (i)) [5]. The obtained results are compared with those obtained from the Sherrington-Kirkpatrick approach using the replica method (method (ii)) [3]. As common features, the phase diagram contains the P, F, M, and SG phases. The shape of the phase diagram depends on the degree exponent λ and is classified based on three cases: $\lambda = \infty$, $3 < \lambda < \infty$, and $2 < \lambda \leq 3$. We note that in our previous work [3], the coupling strength is given stochastically as $J_{ij} = r\delta(J_{ij} - J) + (1 - r)\delta(J_{ij} + J)$, where r serves as the asymmetry ratio between ferromagnetic and antiferromagnetic interactions. Thus, the parameter r plays a similar role to that of J_0/J in the current work, although the two quantities may not be exactly mapped. As different features, there exist two types of phase transitions, the second-order and the first-order transitions in method (i); however, only the second-order phase transition exists in method (ii). In the phase diagram of method (i), the F-SG and F-M phase boundaries are of the first order. However, the transition between the SG and M phases are of the second order. Subsequently, there exists a critical endpoint at which the SG, M, and F phases meet. At this point, the magnetic order parameter exhibits a hybrid phase transition. Moreover, the formulas for the phase boundaries are different. The critical behavior of the SG order parameter depends on the methodology applied.

Thus far, the van Hemmen-type SG models have been investigated as one of the SG solutions [17–21], although their SG phases lack multiplicity of metastable states [22]. According to our work, the present model becomes exactly solvable when the model is on SF networks. The phase diagram and the features of the phase transitions we obtained here would be helpful to understand emerging patterns from socio-complex systems.

ACKNOWLEDGMENTS

This work was supported by Sogang University (Grant No. 201610033.01) and the NRF of Korea (Grant No. 2014R1A3A2069005).

[1] H. Nishimori, *Statistical Physics of Spin Glasses and Information Processing: An Introduction* (Oxford University Press, Oxford, 2001).
[2] T. Nikoletopoulos, A. C. C. Coolen, I. Pérez Castillo, N. S. Skantzos, J. P. L. Hatchett, and B. Wemmenhove, J. Phys. A **37**, 6455 (2004).
[3] D. -H. Kim, G. J. Rodgers, B. Kahng, and D. Kim, Phys. Rev. E **71**, 056115 (2005).
[4] D. -H. Kim, Phys. Rev. E **89**, 022803 (2014).
[5] J. L. van Hemmen, Phys. Rev. Lett. **49**, 409 (1982); J. L. van Hemmen, A. C. D. van Enter, and J. Canisius, Z. Phys. B **50**, 311 (1983).
[6] P. Erdős and A. Rényi, Publ. Math.-Debr. **6**, 290 (1959); Publ. Math. Inst. Hung. Acad. Sci. **5**, 17 (1960).
[7] Bollobás, B. *Random Graphs* (Cambridge University Press, 2001).
[8] K. -I. Goh, B. Kahng, and D. Kim, Phys. Rev. Lett. **87**, 278701 (2001); J. -S. Lee, K. -I. Goh, B. Kahng, and D. Kim, Eur. Phys. J. B **49**, 231 (2006).
[9] D. -S. Lee, K. -I. Goh, B. Kahng, and D. Kim, Nucl. Phys. B **696**, 351 (2004).
[10] D. Grensing and R. Kühn, J. Phys. (Paris) **48**, 713 (1987).
[11] Ph. de Smedt, J. O. Indekeu, and L. Zhang, Physica A **140**, 450 (1987).
[12] S. N. Dorogovtsev, A. V. Goltsev, and J. F. F. Mendes, Phys. Rev. Lett. **96**, 040601 (2006).
[13] G. J. Baxter, S. N. Dorogovtsev, A. V. Goltsev, and J. F. F. Mendes, Phys. Rev. Lett. **109**, 248701 (2012).
[14] A. Bar and D. Mukamel, Phys. Rev. Lett. **112**, 015701 (2014).
[15] S. Jang, J. S. Lee, S. Hwang, and B. Kahng, Phys. Rev. E **92**, 022110 (2015).
[16] W. Cai, L. Chen, F. Ghanbarnejad, and P. Grassberger, Nat. Phys. **11**, 936 (2015).
[17] J. V. Moreira and P. L. Christiano, J. Phys. A **25**, L739 (1992).
[18] T. Celik, U. H. E. Hansmann, and M. Katoot, J. Stat. Phys. **73**, 775 (1993).
[19] Y. Nogueira, J. R. Viana, and J. R. de Sousa, Braz. J. Phys. **37**, 331 (2007).
[20] S. G. Magalhaes, F. M. Zimmer, and C. V. Morais, Phys. Lett. A **374**, 3554 (2010).
[21] F. M. Zimmer, I. C. Berger, and S. G. Magalhaes, Phys. Lett. A **376**, 566 (2012).
[22] T. C. Choy and D. Sherrington, J. Phys. C **17**, 739 (1984).